ADVANCED MATERIALS

lithography process, using the increase in the T_g of the photoresist particles caused by UV-induced crosslinking. Subsequent deposition of silica through the patterned-colloidal mask yielded ordered domains of nanoscale-hole arrays on a micrometer length scale. The present technique produces a spatially organized mask with multiple length scales for colloidal lithography. As such, various functional materials can be deposited through these multiscale colloidal masks, fabricating nanopatterned substrates, which are of practical significance in a wide range of applications from biosensors to optoelectronic devices.

Experimental

Synthesis of Photoresist Particles: MMA (Aldrich, >99 %) and GMA (Aldrich, >95 %) were used as supplied. Potassium persulfate (KPS) was used as an initiator for emulsion polymerization. A 100 mL two-necked round-bottom flask was filled with KPS dissolved in 50 mL of distilled water, and a monomer mixture of MMA and GMA. The content of KPS was fixed at 1 wt.-%. The content of GMA was varied in the range 5–30 wt.-% of the total monomer content, which was fixed at 10 wt.-%. The system was kept under a nitrogen atmosphere and the reaction mixture was stirred magnetically at 300 rpm. When the KPS was dissolved completely, the mixture was heated to 75 °C using an oil bath. After 12 h, the mixture was separated by centrifugation and was purified with distilled water several times. The size of the particles, measured by SEM, ranged from 360 to 420 nm. Later, the cationic photoinitiator, Irgacure 250, was introduced to the photoresist particles by spin-coating.

Measurement of T_g: The glass-transition temperatures of the UV-exposed and UV-screened poly(MMA-*co*-GMA) particles were determined using a differential scanning calorimeter (DSC, TA Instruments, Q1000) under a nitrogen atmosphere at a heating rate of 10 °C min^{-1}. To measure the T_g of UV-exposed particles, the particles were fully baked at 150 °C for 2 h after UV exposure, because the crosslinking reaction could proceed during the DSC measurement. Therefore, the measured T_g could be higher than the T_g of the UV-exposed particles in the patterning. Meanwhile, T_g of the UV-screened particles was compared with that estimated using the rule-of-mixtures theory where T_g= 115 °C for polyMMA and T_g= 75 °C for polyGMA [19].

Deposition of Silica: Silica was deposited in a batch reactor under atmospheric pressure at room temperature. The sample was sequentially exposed to water vapor for 30 min, dried in argon gas for purging the reactor, and then $SiCl_4$ vapor for 20 min. The reactant vapors were carried by argon gas under atmospheric pressure. The concentration of $SiCl_4$ was 0.05 vol.-% in moisture-free argon gas and the relative humidity of water vapor was 50 %. (Caution: silicon tetrachloride is a very corrosive liquid. Use it only with adequate ventilation, and wear protective clothing and safety goggles.) The thickness of the silica layer was controlled by the exposure time to the precursor vapor and around 50 nm for 30 min exposure was obtained.

Received: June 7, 2005
Final version: August 19, 2005
Published online: September 15, 2005

[1] G. L. -T. Chiu, J. M. Shaw, *IBM J. Res. Dev.* **1997**, *41*, 3.
[2] a) H. W. Deckman, J. H. Dunsmir, *Appl. Phys. Lett.* **1982**, *41*, 377. b) T. R. Jensen, M. L. Duval, J. L. Kelly, A. A. Lazarides, G. C. Schatz, R. P. Van Duyne, *J. Phys. Chem. B* **1999**, *103*, 9846. c) C. L. Haynes, R. P. Van Duyne, *J. Phys. Chem. B* **2001**, *105*, 5599.
[3] E. W. Edwards, M. F. Montague, H. H. Solak, C. J. Hawker, P. F. Nealey, *Adv. Mater.* **2004**, *16*, 1315.
[4] J. Peng, Y. C. Han, J. Fu, Y. M. Yang, B. Y. Li, *Macromol. Chem. Phys.* **2003**, *204*, 125.
[5] U. Schmelmer, R. Jorda, W. Geyer, W. Eck, A. Golzhauser, M. Grunze, A. Ulman, *Angew. Chem. Int. Ed.* **2003**, *42*, 559.
[6] a) A. Kosiorek, W. Kandulski, H. Glaczynska, M. Giersig, *Small* **2005**, *1*, 439. b) N. Li, M. Zinke-Allmang, *Jpn. J. Appl. Phys., Part 1* **2002**, *41*, 4626. c) M. E. Abdelsalam, P. N. Bartlett, J. J. Baumberg, S. Coyle, *Adv. Mater.* **2004**, *16*, 90. d) K. Kempa, B. Kimball, J. Rybczynski, Z. P. Huang, P. F. Wu, D. Steeves, M. Sennett, M. Giersig, D. V. G. L. N. Rao, D. L. Carnahan, D. Z. Wang, J. Y. Lao, W. Z. Li, Z. F. Ren, *Nano. Lett.* **2003**, *3*, 13. e) X. D. Wang, E. Graugnard, J. S. King, L. Z. Wang, C. J. Summers, *Nano Lett.* **2004**, *4*, 2223.
[7] C. L. Haynes, A. D. McFarland, M. T. Smith, J. C. Hulteen, R. P. Van Duyne, *J. Phys. Chem. B* **2002**, *106*, 1898.
[8] a) J. Rybczynski, D. Banerjee, A. Kosiorek, M. Giersig, Z. F. Ren, *Nano Lett.* **2004**, *4*, 2037. b) D.-G Choi, H. K. Yu, S. G. Jang, S.-M. Yang, *J. Am. Chem. Soc.* **2004**, *126*, 7019. c) D.-G Choi, S. Kim, E. Lee, S.-M. Yang, *J. Am. Chem. Soc.* **2004**, *127*, 1636.
[9] A. M. Cassel, Q. Ye, B. A. Cruden, J. Li, P. C. Sarrazin, H. T. Ng, J. Han, M. Meyyappan, *Nanotechnology* **2004**, *15*, 9.
[10] E. Chow, S. Y. Lin, S. G. Johnson, P. R. Villeneuve, J. D. Joannopoulos, J. R. Wendt, G. A. Vawter, W. Zubrzycki, H. Hou, A. Alleman, *Nature* **2000**, *407*, 983.
[11] A. Ymeti, J. S. Kanger, J. Grevea, G. A. J. Besselink, P. V. Lambeck, R. Wijn, R. G. Heideman, *Biosens. Bioelectron.* **2005**, *20*, 1417.
[12] a) Y. Yin, Y. Lu, B. Gates, Y. Xia, *J. Am. Chem. Soc.* **2001**, *41*, 8718. b) Z.-Z. Gu, A. Fujishima, O. Sato, *Angew. Chem. Int. Ed.* **2002**, *41*, 2068. c) R. C. Hayward, D. A. Saville, I. A. Aksay, *Nature* **2000**, *404*, 56.
[13] P. Jiang, M. J. McFarland, *J. Am. Chem. Soc.* **2005**, *127*, 3710.
[14] J. H. Moon, W. S. Kim, J.-W. Ha, S. G. Jang, S.-M. Yang, J.-K. Park, *Chem. Commun.* **2005**, 4107.
[15] J. H. Glans, D. T. Turner, *Polymer* **1981**, *22*, 1540.
[16] M. Okubo, Y. Nakamura, T. Matsumoto, *J. Polym. Sci., Polym. Chem. Ed.* **1980**, *18*, 2451.
[17] A. S. Dimitrov, K. Nagayama, *Langmuir* **1996**, *12*, 1303.
[18] J. P. Fouassier, *Photoinitiation, Photopolymerization and Photocuring*, Hansen Publishers, Munich **1995**.
[19] H. A. Schneider, J. Rieger, E. Penzel, *Polymer* **1997**, *38*, 1323.

One-Pot Synthesis of Octahedral Cu_2O Nanocages via a Catalytic Solution Route**

By *Conghua Lu*, *Limin Qi*,* *Jinhu Yang*, *Xiaoyu Wang*, *Dayong Zhang*, *Jinglin Xie*, and *Jiming Ma*

In recent years there has been increasing interest in the controlled synthesis of inorganic micro- and nanostructures with hollow interiors because of their widespread potential appli-

[*] Prof. L. Qi, Dr. C. Lu, Dr. J. Yang, X. Wang, D. Zhang, J. Xie, Prof. J. Ma
State Key Laboratory for Structural Chemistry of Unstable and Stable Species
College of Chemistry, Peking University
Beijing, 100871 (P.R. China)
E-mail: liminqi@pku.edu.cn

[**] This work was supported by NSFC (20 325 312, 20 473 003, and 20 233 010) and FANEDD (200 020). The authors thank Prof. Nianzu Wu for help on the XPS measurements. Supporting Information is available online from Wiley InterScience or from the authors.

  DOI: 10.1002/adma.200501128

cations, including as catalysts, adsorbents, sensors, photonic crystals, drug-delivery carriers, biomedical diagnosis agents, lightweight fillers, acoustic insulators, and chemical reactors.[1–6] Among the many synthetic routes to inorganic hollow structures, template-directed synthesis, where hard templates, such as polymer latex particles,[1] silica spheres,[7] metal nanoparticles,[8] and carbon spheres,[9] and soft templates, such as emulsion droplets,[10,11] micelles,[12] and gas bubbles,[13] are employed as removable templates, has been demonstrated to be an effective approach. The direct self-assembly of building blocks without external templates has also been utilized for generating hollow structures.[14,15] Notably, hollow nanocrystals of cobalt oxide and chalcogenides,[3] hollow ZnO dandelions,[16] and hollow Pb/PbS particles[17] have been prepared through the Kirkendall effect by using spherical Co, Zn, and Pb particles as sacrificial templates, respectively. However, the hollow structures obtained are mostly spherical, polycrystalline shells consisting of primary particles. Since the properties of inorganic hollow structures may be well tuned by tailoring their morphology and crystallinity, some recent efforts have been devoted to the synthesis of inorganic hollow structures with well-defined non-spherical morphologies. In particular, cubic Au–Ag alloy nanoboxes with a single-crystalline nature were synthesized through a galvanic replacement reaction by using silver nanocubes as templates,[2,18] whereas micrometer-sized rhombododecahedral Ag cages with a hierarchical structure were prepared through the Kirkendall effect by using rhombododecahedral Ag_3PO_4 crystals as precursor templates.[5] Moreover, polycrystalline hollow SnO_2 octahedra were produced by a one-pot solution route based on the two-dimensional aggregation of nanocrystallites.[4] In addition, polyhedral, single-crystalline hollow ZnO beads were obtained via a solid–vapor deposition process[19] and also via a laser-assisted growth process.[20] However, it remains a great challenge to develop feasible methods for the one-pot, template-free, solution synthesis of single-crystalline cages with well-defined non-spherical morphologies.

As a p-type semiconductor (direct bandgap ~2.17 eV) with unique optical and magnetic properties, cuprous oxide (Cu_2O) is a promising material with potential applications in solar energy conversion, micro-/nanoelectronics, magnetic storage devices, catalysis, and biosensing.[21–23] Moreover, Cu_2O crystals have been at the center of research on the Bose–Einstein condensation of excitons.[24] Many recent efforts have been devoted to the shape-controlled synthesis of Cu_2O micro- and nanocrystals. Systematic manipulation of the morphology and architecture of Cu_2O microcrystals has been achieved using solution routes[25–27] and electrodeposition methods.[28] Meanwhile, various approaches have been reported for fabricating Cu_2O nanocrystals with varied morphologies, such as wires,[29] cubes,[30,31] pyramids,[31] and octahedra.[32] In particular, monodisperse Cu_2O nanocubes ranging in edge length from 200 to 450 nm have been synthesized in an aqueous cetyltrimethylammonium bromide solution.[30] It was observed that the nanocubes were made of smaller particles and had a partially hollow interior; however, the formation mechanism of the empty interiors remained unclear. Cu_2O cubes with hollow interiors have also been obtained by the preparation of relatively large Cu_2O nanocubes (~500 nm in edge length), followed by their separation and dispersion in acetic acid solution.[33] Recently, polycrystalline hollow Cu_2O nanospheres (100–200 nm in outer diameter) with variable bandgap energy (E_g) in the range 2.405–2.170 eV have been fabricated via a reductive transformation of the aggregated CuO nanocrystallites and a subsequent Ostwald ripening process, without using templates.[23] Since single-crystalline Cu_2O nanostructures with tailored architectures are expected to show novel properties,[22] it would be desirable to fabricate single-crystalline hollow Cu_2O nanocages with modulated morphologies. Herein, we report a facile one-pot solution synthesis of uniform single-crystalline octahedral Cu_2O nanocages by a catalytic self-templating route without using pre-fabricated templates. A wealth of colorful Cu_2O nanostructures with widely tunable E_gs in the range 2.6–2.2 eV have been prepared by the catalytic reduction of copper tartrate complex into Cu_2O nanooctahedra, followed by their catalytic oxidative evacuation.

The reaction for reducing the copper tartrate complex (Fehling's solution) with glucose to form a Cu_2O precipitate, which is widely used in the analytical determination of saccharides, has been adapted to prepare uniform micrometer-sized Cu_2O octahedra (1.0–1.6 μm) by McFadyen and Matijevic in the 1970s.[25] On the other hand, Fehling's solution has been frequently used for the electroless plating of copper on surfaces activated by $PdCl_2$, which is reduced to Pd metal in the copper-plating bath to act as a catalyst for the subsequent electroless deposition of copper.[34,35] Here, $PdCl_2$ has been introduced into the reaction mixture of Fehling's solution and the reductant glucose for the catalytic solution synthesis of unique octahedral Cu_2O nanocages. A typical scanning electron microscopy (SEM) image of the Cu_2O crystals obtained after 3 h of aging at 75 °C is shown in Figure 1a, which suggests that the product exhibits uniform, regular octahedra with an average edge length of ~230 nm. The well-defined octahedral morphology with a cubic symmetry is characteristic of single-crystalline cubic-structured Cu_2O crystals bound by eight {111} planes (Fig. 1b). It can also be observed in Figure 1a that the nanooctahedra usually have holes on the apexes, and that some partially broken particles clearly show a hollow interior, indicating the formation of octahedral Cu_2O nanocages. The X-ray diffraction (XRD) pattern (Fig. S1a, Supporting Information) suggests that the octahedral nanocages are actually pure Cu_2O crystals with a cubic structure (Joint Committee on Powder Diffraction Standards (JCPDS) Card No. 05-0667). Furthermore, X-ray photoelectron spectroscopy (XPS), which is very sensitive to the oxidation state of copper (e.g., Cu^{2+}, Cu^{+}, and Cu^{0}), has been used to characterize the product. As shown in Figure S1b (Supporting Information), the binding energies of the photoelectron peaks at 932.4 ($Cu\,2p_{3/2}$) and 952.3 eV ($Cu\,2p_{1/2}$) together with the kinetic energy (KE) of the Cu(L_3VV) Auger peak at 916.5 eV are characteristic of the Cu_2O phase,[36] confirming

ADVANCED MATERIALS

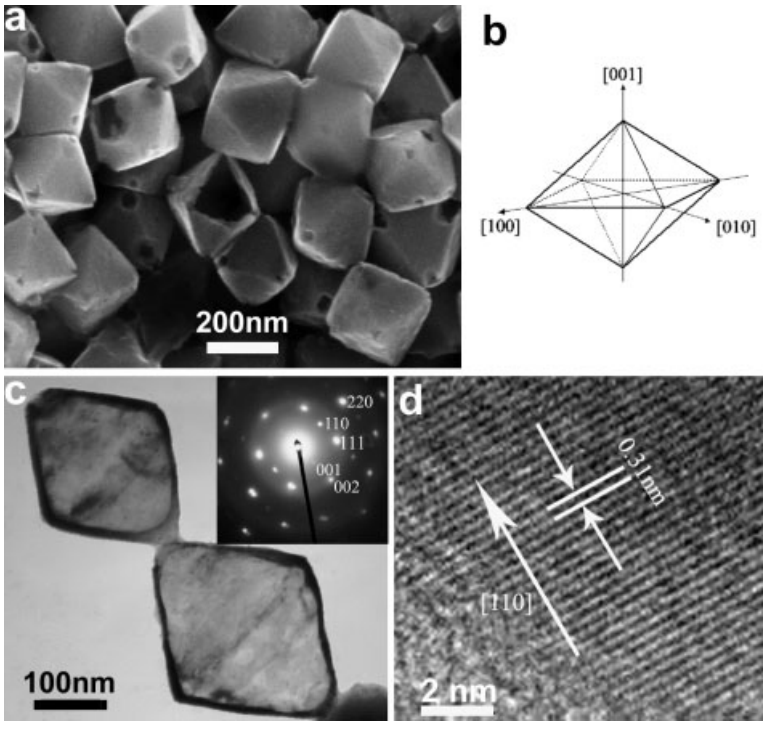

Figure 1. a) SEM image of octahedral Cu_2O nanocages obtained at an aging time of 3 h. b) Schematic illustration of an octahedral Cu_2O crystal. c) TEM and d) HRTEM images of octahedral Cu_2O nanocages obtained at an aging time of 3 h. The inset to (c) shows the SAED pattern of the upper Cu_2O nanocage.

the formation of pure Cu_2O crystals. Figure 1c shows a typical transmission electron microscopy (TEM) image of the Cu_2O product, which suggests that the octahedral particles are actually octahedral nanocages with a wall thickness typically in the 10–14 nm range. The selected area electron diffraction (SAED) pattern corresponding to a single nanocage showing a rhombic projection can be indexed to the $[1\bar{1}0]$ zone axis of cubic-structured Cu_2O with a (001) direction along the longer diagonal direction of the rhomb. This indicates that this octahedral nanocage is a single crystal of Cu_2O with a [110]-oriented edge lying on the substrate by accident. The single-crystalline nature of the nanocages has been further demonstrated by the high-resolution TEM (HRTEM) image shown in Figure 1d, which exhibits clear fringes attributed to the (110) planes of Cu_2O. To the best of our knowledge, this is the first synthesis of single-crystalline Cu_2O nanocages with well-defined octahedral morphology.

To shed light on the formation mechanism of these novel octahedral Cu_2O nanocages, their growth process has been followed by examining the products harvested at different intervals of aging times. Figure 2 shows representative SEM and TEM images of the products obtained after various aging times, which have been demonstrated to be pure Cu_2O crystals by related XRD measurements, excluding the presence of CuO and Cu crystals in the products. As shown in Figure 2a, quasi-octahedral solid nanoparticles (~130 nm in edge length) with rugged surfaces are obtained after aging for 5 min. After aging for 25 min, larger octahedral nanocrystals (~230 nm in edge length) with slightly rough surfaces are produced (Fig. 2b). When the aging time is increased to 2 h, octahedral crystals of a similar size (~230 nm in edge length) with smooth surfaces appear, which show holes on the apexes as well as pores in the interiors (Fig. 2c), indicating the formation of partially hollow nanooctahedra due to an evacuation process from the apexes. Upon gradual evacuation of the interior, well-defined octahedral nanocages are produced after an aging time of 3 h, as shown in Figure 1. Notably, the octahedral nanocages are gradually etched into fragments when the aging time is further prolonged and irregular nanoparticles, about tens of nanometers in size, are obtained at an aging time of 6 h (Fig. 2d). The Cu_2O particles are totally dissolved after 10 h of aging, resulting in a transparent light-blue solution, similar to the original reaction solution containing the copper tartrate complex.

A series of color changes have been observed in the reaction solution accompanying the evolution of the Cu_2O product in size and morphology. The UV-vis spectra shown in Figure 3a suggests that the original solution of the Cu^{2+}–tartrate complex shows only a weak broad absorption in the 600–800 nm range. After aging at 75 °C for 2.5 min, an absorption peak around 485 nm emerges owing to the formation of Cu_2O particles. The absorption peak gradually red-shifts to ~560 nm as the aging time increases to 30 min, with the evolution of the initial smaller particles into well-developed octahedral nanocrystals (~230 nm in edge length). As the aging process continues, the evacua-

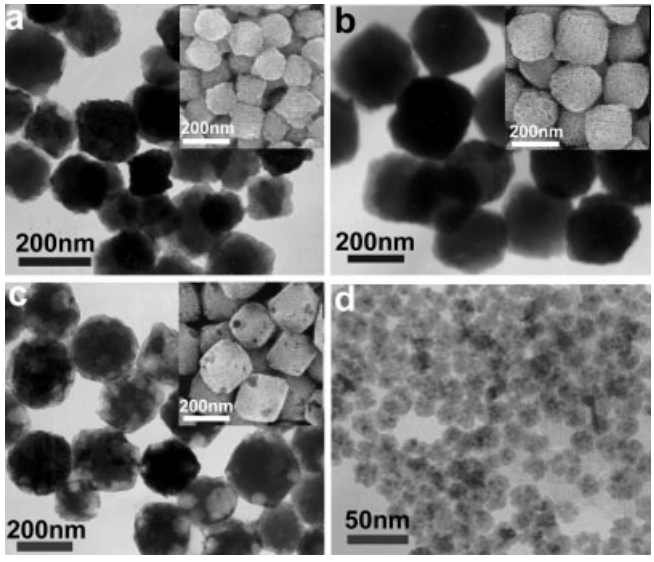

Figure 2. TEM images of Cu_2O products obtained at different aging times: a) 5 min, b) 25 min, c) 2 h, and d) 6 h. Insets: the corresponding SEM images.

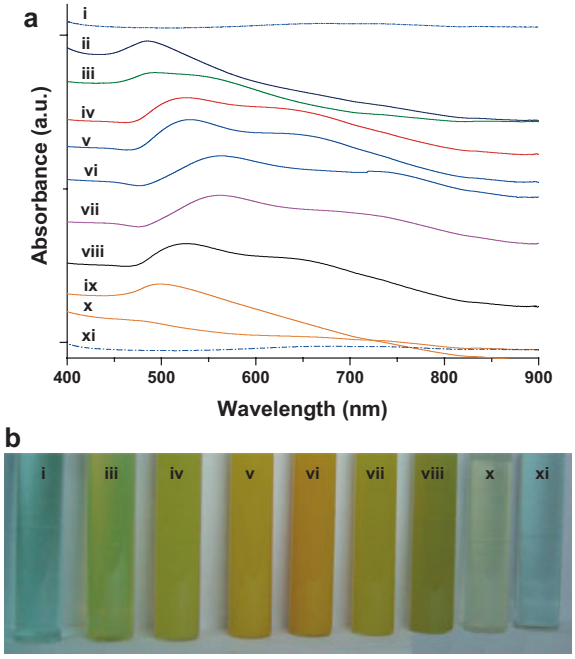

Figure 3. a) UV-vis spectra and b) optical color evolution of Cu_2O products, obtained at different aging times: i) 0 min, ii) 2.5 min, iii) 5 min, iv) 10 min, v) 15 min, vi) 30 min, vii) 1.5 h, viii) 3 h, ix) 4 h, x) 7 h, and xi) 10 h.

tion process takes place, leading to a gradual blue-shift of the absorption peak. In particular, the well-defined octahedral Cu_2O nanocages obtained at an aging time of 3 h exhibit an absorption peak at ~526 nm. With further aging, the absorption peak owing to Cu_2O crystals blue-shifts and finally disappears, while a weak broad peak around 600–800 nm appears again, indicating the gradual oxidative dissolution of Cu_2O crystals into the soluble Cu^{2+}–tartrate complex. As a result, the color of the reaction solution varies from light blue to brown–red, and back to light blue with aging time (Fig. 3b). This result indicates that the optical bandgaps of Cu_2O nanostructures can be fine-tuned in the range 2.6–2.2 eV, which is considerably wider than the bandgap range observed for the hollow Cu_2O nanospheres showing a wealth of colors, i.e., 2.4–2.2 eV.[23] Moreover, well-resolved absorption peaks have been observed for the current Cu_2O nanostructures, whereas absorption shoulders were usually observed for the reported hollow Cu_2O nanospheres. In general, the optical absorption of Cu_2O nanocrystallites should blue-shift from the absorption of bulk Cu_2O, which is ~570 nm (bandgap ~2.17 eV), with decreasing crystallite size as a result of quantum size effects. Although a quantum-confinement threshold was once deduced to be 14 nm for Cu_2O nanocrystallites,[23] the optical absorption would be affected considerably by the morphology and crystallinity of Cu_2O crystals. For example, an absorption peak at 482 nm was reported for octahedral Cu_2O nanocrystals with an edge length of 95 nm.[32] Therefore, our observations on the tunable optical absorption of Cu_2O nanostructures may be rationalized by considering that the blue-shift of the absorption of octahedral Cu_2O nanocrystals can be achieved in two different ways, i.e., by a decrease in the overall crystal size or by a hollowing of the crystals. In other words, the initial red-shift in the absorption with aging time may be attributed to an increase in the size of the octahedral crystals (up to ~230 nm in edge length), while the subsequent blue-shift with aging time can be largely attributed to the hollowing of the octahedral crystals, which results in the formation of octahedral nanocages with a wall thickness of about 10–14 nm.

Based on the examination of the time-dependent formation of octahedral Cu_2O nanocages, we propose that the octahedral nanocages are formed by a two-step process, i.e., the formation of octahedral solid nanocrystals by the Pd^0-catalyzed reduction of the copper tartrate complex with glucose, followed by the subsequent hollowing of the nanooctahedra by a Pd^0-catalyzed, oxygen-engaged oxidation process. During the first step, $PdCl_2$ may be reduced to small Pd^0 nanoparticles by glucose prior to the reduction of the Cu^{2+}–tartrate complex; Pd^0 then acts as a catalyst for the reductive transformation of Cu^{2+} to Cu_2O particles, similar to the electroless copper plating process activated by $PdCl_2$. During the second step, the trace oxygen dissolved in solution may gradually oxidize Cu_2O into Cu^{2+} in the presence of the Pd^0 catalyst, which is supported by the observation that the oxidative etching process is effectively prevented when N_2 is purged into the solution to remove dissolved O_2 prior to the reaction. It is believed that the Pd^0 catalyst plays an important role in the selective etching of the octahedral apexes and the preferential evacuation of the octahedra. Since the adsorption of tartrate ions on the surfaces of the octahedra could considerably prevent direct contact with the Pd^0 catalyst, preferential oxidative etching of the apexes of the Cu_2O octahedra would occur due to their relatively higher activity. Subsequently, dissolved oxygen together with the Pd^0 catalyst would continue to diffuse into the interior through the open corners, resulting in a gradual hollowing of the octahedra. A control experiment conducted without adding $PdCl_2$ provides support for the proposed mechanism. As shown in Figure S2a (Supporting Information), rather larger Cu_2O octahedra (~600 nm in edge length) have been obtained after 30 min of aging in the absence of $PdCl_2$, suggesting the role of the Pd^0 catalyst in producing smaller octahedra. Moreover, partially etched octahedra have been obtained at an aging time of 24 h; however, the etching occurs mainly on the surfaces of the octahedra, and hollowing of the octahedra does not occur (Fig. S2b, Supporting Information).

For comparison purposes, the synthesis experiment has also been carried out in the presence of poly(vinyl pyrrolidone) (PVP), a typical polymeric protector for Pd nanoparticles. A representative SEM image shown in Figure 4a suggests that uniform corner-etched Cu_2O octahedra that are about 200 nm in size have been produced, which is in good contrast to the interior-etched octahedral nanocages obtained without adding PVP. An enlarged image shows that the etched corner looks like a pyramidal pit with a regular square opening, which mir-

ADVANCED MATERIALS

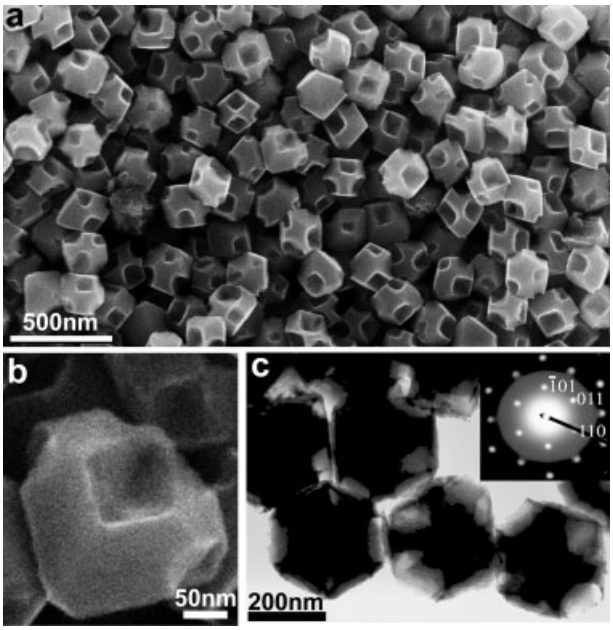

Figure 4. a,b) SEM and c) TEM images of corner-etched Cu_2O octahedra obtained at an aging time of 3 h in the presence of PVP. Inset: the related SAED pattern.

rors the cubic crystal symmetry (Fig. 4b). The TEM image shown in Figure 4c is consistent with the corner-etched structure of the octahedral particles while the SAED pattern corresponding to a single octahedron confirms its single-crystalline nature. This observation may be rationalized by considering that the adsorption of PVP on the Pd catalyst could impair its catalytic activity and slow down the oxidative dissolution of Cu_2O through the open corners, resulting in a gradual widening of the open corners. This speculation is supported by the experimental observation that even in the presence of PVP, octahedral Cu_2O nanocages can also be obtained after an appropriate aging time if a larger amount of $PdCl_2$ is added to the solution. In addition, the specific adsorption of PVP on different crystal faces of the octahedral Cu_2O crystals may somewhat change the surface free energies and thus contribute to a slowing down of the oxidative dissolution of Cu_2O through the open corners.

In conclusion, uniform single-crystalline octahedral Cu_2O nanocages that are about 230 nm in edge length have been synthesized by a novel one-pot catalytic solution route, which involves the formation of octahedral Cu_2O nanocrystals and a subsequent spontaneous hollowing process. A wealth of colorful Cu_2O nanostructures with widely tunable bandgaps in the range of 2.6–2.2 eV have been obtained by this synthetic route. This facile one-pot approach to inorganic hollow structures with novel morphologies could be potentially extended to other inorganic systems. The obtained octahedral Cu_2O nanocages may find potential applications in solar energy conversion, catalysis, and as model systems for fundamental research.

Experimental

Octahedral Cu_2O nanocages were prepared via the catalytic reduction of a basic copper tartrate complex solution (Fehling's solution) with glucose followed by an oxygen-engaged catalytic oxidation process. A stock Fehling's solution composed of 7 g L^{-1} of $CuSO_4 \cdot 5H_2O$, 25 g L^{-1} of potassium sodium tartrate tetrahydrate, and 4.5 g L^{-1} of KOH was first prepared. In a typical synthesis of Cu_2O nanocages, 0.01 mL $PdCl_2$ (0.027 M) and 0.1 mL glucose (0.25 M) solutions were added successively into a mixed solution of 0.5 mL of the stock Fehling's solution and 4.5 mL of water under stirring, resulting in a clear light-blue solution, which was then aged at 75 °C under static conditions for 3 h. The precipitates were separated by centrifugation at 3000 revolutions per minute (rpm), washed thoroughly with water, and dried under vacuum overnight. For comparison purposes, the synthesis was also conducted in the absence of $PdCl_2$ or in the presence of 5 mM PVP (weight-average molecular weight, $M_w = 30\,000$, Aldrich) as an additive. The obtained products were characterized by field-emission scanning electron microscopy (AMRY 1910), TEM (JEOL JEM-200CX), HRTEM (Tecnai F30), XRD (Rigaku Dmax-2000 with Cu Kα radiation), XPS (Kratos Axis Ultra spectrometer with monochromatized Al Kα radiation), and UV-vis spectroscopy (CaryIE, Varian). To follow the evolution of the optical absorption of the Cu_2O products with aging time, UV-vis spectra of the mixed solution were measured directly at room temperature after the solution was aged at 75 °C for varied periods. It was noted that the absorption spectra obtained from the dispersion formed by redispersing separated Cu_2O nanostructures in water were essentially the same as the spectra measured in situ from the mixed solution.

Received: June 1, 2005
Final version: June 27, 2005
Published online: September 15, 2005

[1] F. Caruso, R. A. Caruso, H. Möhwald, *Science* **1998**, *282*, 1111.
[2] Y. Sun, Y. Xia, *Science* **2002**, *298*, 2176.
[3] Y. Yin, R. M. Rioux, C. K. Erdonmez, S. Hughes, G. A. Somorjai, A. P. Alivisatos, *Science* **2004**, *304*, 711.
[4] H. G. Yang, H. C. Zeng, *Angew. Chem. Int. Ed.* **2004**, *43*, 5930.
[5] J. Yang, L. Qi, C. Lu, J. Ma, H. Cheng, *Angew. Chem. Int. Ed.* **2005**, *44*, 598.
[6] J. Chen, F. Saeki, B. J. Wiley, H. Cang, M. J. Cobb, Z.-Y. Li, L. Au, H. Zhang, M. B. Kimmey, X. Li, Y. Xia, *Nano Lett.* **2005**, *5*, 473.
[7] S.-W. Kim, M. Kim, W. Y. Lee, T. Hyeon, *J. Am. Chem. Soc.* **2002**, *124*, 7642.
[8] H.-P. Liang, H.-M. Zhang, J.-S. Hu, Y.-G. Guo, L.-J. Wan, C.-L. Bai, *Angew. Chem. Int. Ed.* **2004**, *43*, 1540.
[9] X. Sun, Y. Li, *Angew. Chem. Int. Ed.* **2004**, *43*, 3827.
[10] B. Z. Putlitz, K. Landfester, H. Fischer, M. Antonietti, *Adv. Mater.* **2001**, *13*, 500.
[11] J. Bao, Y. Liang, Z. Xu, L. Si, *Adv. Mater.* **2003**, *15*, 1832.
[12] D. Zhang, L. Qi, J. Ma, H. Cheng, *Adv. Mater.* **2002**, *14*, 1499.
[13] Q. Peng, Y. Dong, Y. Li, *Angew. Chem. Int. Ed.* **2003**, *42*, 3027.
[14] A. Bigi, E. Boanini, D. Walsh, S. Mann, *Angew. Chem. Int. Ed.* **2002**, *41*, 2163.
[15] B. Liu, H. C. Zeng, *J. Am. Chem. Soc.* **2004**, *126*, 8124.
[16] B. Liu, H. C. Zeng, *J. Am. Chem. Soc.* **2004**, *126*, 16 744.
[17] Y. Wang, L. Cai, Y. Xia, *Adv. Mater.* **2005**, *17*, 473.
[18] Y. Sun, Y. Xia, *J. Am. Chem. Soc.* **2004**, *126*, 3892.
[19] P. X. Gao, Z. L. Wang, *J. Am. Chem. Soc.* **2003**, *125*, 11 299.
[20] Z.-Y. Jiang, Z.-X. Xie, X.-H. Zhang, S.-C. Lin, T. Xu, S.-Y. Xie, R.-B. Huang, L.-S. Zheng, *Adv. Mater.* **2004**, *16*, 904.
[21] X. Li, H. Gao, C. J. Murphy, L. Gou, *Nano Lett.* **2004**, *4*, 1903.
[22] R. Liu, E. A. Kulp, F. Oba, E. W. Bohannan, F. Ernst, J. A. Switzer, *Chem. Mater.* **2005**, *17*, 725.

[23] Y. Chang, J. J. Teo, H. C. Zeng, *Langmuir* **2005**, *21*, 1074.
[24] D. Snoke, *Science* **2002**, *298*, 1368.
[25] P. McFadyen, E. Matijevic, *J. Colloid Interface Sci.* **1973**, *44*, 95.
[26] D. Wang, M. Mo, D. Yu, L. Xu, F. Li, Y. Qian, *Cryst. Growth Des.* **2003**, *3*, 717.
[27] Y. Chang, H. C. Zeng, *Cryst. Growth Des.* **2004**, *4*, 273.
[28] a) M. J. Siegfried, K.-S. Choi, *Adv. Mater.* **2004**, *16*, 1743. b) M. J. Siegfried, K.-S. Choi, *Angew. Chem. Int. Ed.* **2005**, *44*, 3218.
[29] W. Wang, G. Wang, X. Wang, Y. Zhan, Y. Liu, C. Zheng, *Adv. Mater.* **2002**, *14*, 67.
[30] L. Gou, C. J. Murphy, *Nano Lett.* **2003**, *3*, 231.
[31] R. Liu, F. Oba, E. W. Bohannan, F. Ernst, J. A. Switzer, *Chem. Mater.* **2003**, *15*, 4882.
[32] P. He, X. Shen, H. Gao, *J. Colloid Interface Sci.* **2005**, *284*, 510.
[33] Z. Wang, X. Chen, J. Liu, M. Mo, L. Yang, Y. Qian, *Solid State Commun.* **2004**, *130*, 585.
[34] G. H. Yang, E. T. Kang, K. G. Neoh, Y. Zhang, K. L. Tan, *Langmuir* **2001**, *17*, 211.
[35] W. Prissanaroon, N. Brack, P. J. Pigram, P. Hale, P. Kappen, J. Liesegang, *Thin Solid Films* **2005**, *477*, 131.
[36] J. F. Moulder, W. F. Stickle, P. E. Sobol, K. D. Bomben, *Handbook of X-ray Photoelectron Spectroscopy*, Perkin-Elmer Corporation Physical Electronics Division, Eden Prairie, MN **1992**.

Photoembossing of Periodic Relief Structures Using Polymerization-Induced Diffusion: A Combinatorial Study**

By *Carlos Sánchez*, *Berend-Jan de Gans*, *Dimitri Kozodaev*, *Alexander Alexeev*, *Michael J. Escuti*, *Chris van Heesch*, *Thijs Bel*, *Ulrich S. Schubert*, *Cees W. M. Bastiaansen*,* and *Dirk J. Broer*

Polymeric relief microstructures are extensively used in biosensors, cell-growth arrays, and as microelectronic and microoptical elements in displays.[1–4] To generate these structures, replication methods based on physical contact are used, like embossing or cast-molding. In case of embossing, relief features are transferred by pressing a polymer film against a microstructured rigid master.[5,6] Cast-molding uses a polymer precursor that is poured onto a master, cured, and released to obtain an inverse replica.[7] Relief microstructures can also be made by lithography via a light-induced solubility change of a polymeric photoresist.[8] A wet-etching step develops the final relief structure. Recently, a new solvent-free photolithographic technique was proposed to prepare surface-relief structures.[9–11] The process that we will refer to as "photoembossing" is schematically shown in Figure 1. A photopolymer blend comprising a polymeric binder, a multireactive acrylate, and a photoinitiator is processed as a solid thin film onto a substrate. An irradiation step through a lithographic mask at room temperature (RT) generates radicals in the exposed areas. The photopolymer blend is glassy at RT, which allows the use of contact masks. Monomer diffusion and polymerization are inhibited at this stage, and a free-radical latent image of the mask is formed. A subsequent heating step enhances monomer mobility and polymerization in the irradiated areas. Consumption of monomer in these regions leads to a net flux of unreacted monomer from the unexposed to the exposed areas, resulting in a surface deformation whose final shape is determined by diffusion and surface tension. Photoembossing does not involve any wet developing step, and the mask can directly contact the photopolymer. Therefore, photoembossing is also very attractive from an industrial standpoint.[11]

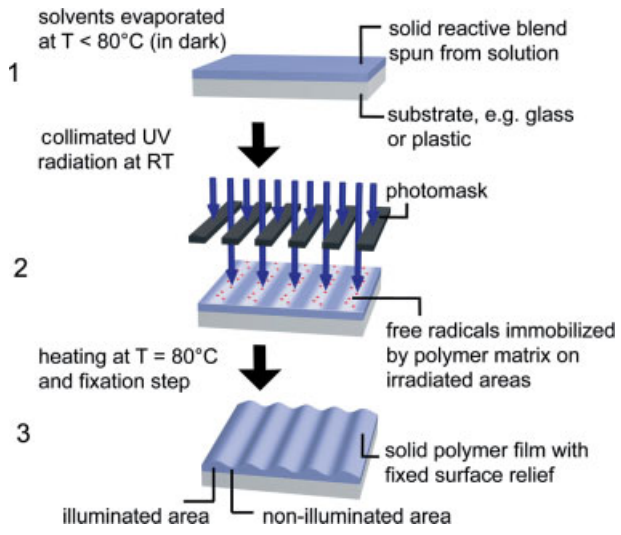

Figure 1. Schematic representation of the photoembossing process. RT, room temperature.

A large variety of processing parameters influence the height and shape of the final relief structure, which determine its performance in specific applications. In this paper, we report on a combinatorial study on the influence of the structure period, energy dose, development temperature, film thickness, and photopolymer blend composition. Automated atomic force microscopy (AFM) is used to characterize the topography of the relief structures with high reproducibility and com-

[*] Dr. C. W. M. Bastiaansen, Dr. C. Sánchez, Dr. B.-J. de Gans, Dr. D. Kozodaev, Dr. A. Alexeev, Dr. M. J. Escuti, C. van Heesch, Prof. U. S. Schubert, Prof. D. J. Broer
Eindhoven University of Technology, Dutch Polymer Institute (DPI)
P.O. Box 902, NL-5600 AX Eindhoven (The Netherlands)
E-mail: c.w.m.bastiaansen@tue.nl
T. Bel, Prof. D. J. Broer
Philips Research Laboratories
Prof. Holstlaan 4, NL-5656 AA Eindhoven (The Netherlands)

[**] The research of Carlos Sánchez, Berend-Jan de Gans, Dimitri Kozodaev, Alexander Alexeev, Michael J. Escuti, Chris van Heesch, Ulrich S. Schubert, Cees W. M. Bastiaansen, and Dirk J. Broer forms part of the research program of the Dutch Polymer Institute (DPI).

 DOI: 10.1002/adma.200500777